J. Plasma Physics (2006), *vol.* 72, *part* 4, *pp.* 443–456. © 2005 Cambridge University Press
doi:10.1017/S0022377805004113 First published online 7 December 2005 Printed in the United Kingdom

Analytical solutions for minimum dissipation states: flux core spheromak sustained by helicity injection

SEBASTIAN BOUZAT and RICARDO FARENGO

Unidad de Actividad de Física, Centro Atómico Bariloche (CNEA) and Instituto Balseiro (CNEA and UNC), 8400 San Carlos de Bariloche, Argentina (bouzat@cab.cnea.gov.ar)

(Received 21 February 2005 and accepted 1 August 2005)

Abstract. Analytical solutions for the minimum Ohmic dissipation states satisfying helicity balance in a cylindrical vessel with circular electrodes on the plane surfaces are presented. The solutions show the basic features of flux core spheromaks and are given in terms of Fourier–Bessel series. The total plasma current and magnetic field profiles are determined for different values of resistivity, elongation and electrode radius.

1. Introduction

Many variational principles have been proposed for calculating relaxed states of weakly turbulent plasmas under different conditions of interest for controlled fusion. A pioneering work in this area is that by Taylor (1974) where the minimum-energy principle was successfully used to explain the basic features of the magnetic field profiles in reversed field pinches (RFP). Two related principles, the minimum rate of entropy production (Hameiri and Bhattacharjee 1987) and the minimum rate of energy dissipation, have been proposed for systems sustained by external fields and currents. The minimum rate of energy dissipation principle was applied to study RFPs in configurations sustained by inductive electric fields (Montgomery and Phillips 1988a, b; Wang and Bhattacharjee 1991), tokamaks (Farengo and Sobehart 1993), tokamaks sustained by helicity injection (Farengo and Sobehart 1994; Caputi and Farengo 2001) and flux core spheromaks (FCS; Farengo and Caputi 2002).

The results presented in Farengo and Caputi (2002) were essentially numerical. In this work we continue with the study of minimum-energy dissipation states in FCS. The main achievement of this work is the development of analytical solutions for the minimum dissipation states in cylindrical vessels with helicity injection that show the basic features of FCSs. The analytical treatment allows us to explore a relatively wide region of parameters of interest and to compare the different states. The solutions could serve as a basis for further studies on the stability and decay of spheromak configurations.

We assume that the viscous dissipation is negligible compared to the Ohmic one, and focus on the minimization of the latter contribution. We calculate the minimum Ohmic dissipation states inside a cylindrical vessel of radius a and length $2L$, with

https://doi.org/10.1017/S0022377805004113 Published online by Cambridge University Press

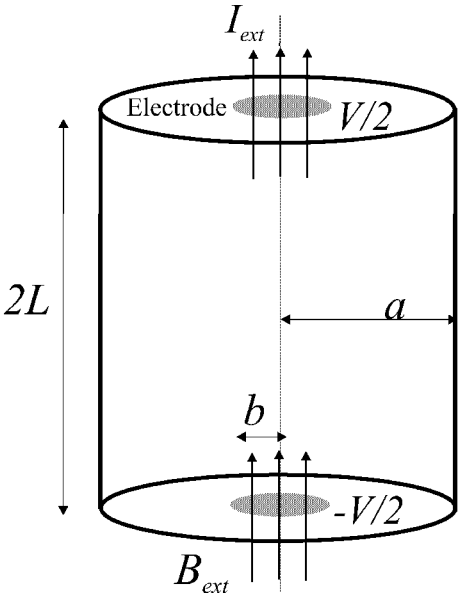


Figure 1. Sketch of the configuration considered.

circular electrodes of radius b on the plane surfaces, as shown in Fig. 1. The two electrodes are kept at voltages $\pm V/2$, and a uniform external magnetic field $\mathbf{B}_{\rm ext}$ is embedded through them. Except for the electrodes, the interior walls of the vessel are assumed to be covered by a non-conducting material.

Helicity balance is satisfied by imposing equal helicity injection ($\dot{K}_{\rm inj}$) and helicity dissipation ($\dot{K}_{\rm dis}$) rates, which are given by (Farengo and Caputi 2002)

$$\dot{K}_{\rm inj} = \int_{S_{\rm electrodes}} \Phi \mathbf{B} \cdot \mathbf{ds}, \quad \dot{K}_{\rm dis} = \int \eta \mathbf{J} \cdot \mathbf{B}\, d^3r, \tag{1.1}$$

where Φ is the potential on the electrodes and η is the resistivity (assumed to be uniform over the whole vessel).

The paper is organized as follows. In Sec. 2 we present the variational principle, the Euler–Lagrange equations and their general solutions. In Sec. 3 we analyze the solutions for $b = 1$ (the case where the electrodes cover the entire plane surfaces of the vessel). In Sec. 4 we present the analytical solutions for $b < 1$. Section 5 contains the summary and conclusions.

2. Variational principle and Euler–Lagrange equations

We search for the minimum dissipation states satisfying helicity balance inside the cylindrical vessel described in the introduction and shown in Fig. 1.

The variational principle is $\delta W = 0$, where

$$W = \int \eta J^2\, d^3r - \frac{\lambda}{\mu_0}\left(\int \eta \mathbf{J} \cdot \mathbf{B}\, d^3r + \int_{S_{\rm electrodes}} \Phi \mathbf{B} \cdot \mathbf{d}s\right)$$
$$- \int \gamma \nabla \cdot \mathbf{B}\, d^3r + \int \mathbf{C} \cdot (\mu_0 \mathbf{J} - \nabla \times \mathbf{B})\, d^3r. \tag{2.1}$$

https://doi.org/10.1017/S0022377805004113 Published online by Cambridge University Press

Here, the first term is the Ohmic dissipation, the term proportional to the Lagrange multiplier λ contains the constraint of helicity balance (Farengo and Caputi 2002); γ and $\mathbf{C}$ are the space-dependent Lagrange multipliers associated with the constraint $\nabla \cdot \mathbf{B} = 0$ and Ampere's law, respectively. The resulting Euler–Lagrange equations are:

$$\begin{gathered}\nabla \cdot \mathbf{B} = 0,\\ \nabla \times \mathbf{B} = \mu_0 \mathbf{J},\\ \frac{\lambda\eta}{\mu_0}\mathbf{B} - 2\eta\mathbf{J} - \mu_0\mathbf{C} = 0,\\ \frac{\lambda\eta}{\mu_0}\mathbf{J} - \nabla\gamma + \nabla\times\mathbf{C} = 0.\end{gathered} \tag{2.2}$$

By combining the last three equations we obtain

$$\nabla\times\mathbf{J} - \lambda\mathbf{J} + \frac{\mu_0}{2\eta}\nabla\gamma = 0. \tag{2.3}$$

The condition $\nabla \cdot \mathbf{J} = 0$ implies

$$\nabla^2\gamma = 0. \tag{2.4}$$

Note that it is not necessary to include the condition $\nabla \cdot \mathbf{J} = 0$ on the variational principle because it results from Ampere's law.

Following procedures similar to those in Farengo and Caputi (2002) and Wang and Bhattacharjee (1991), from the surface terms in the variation of W we obtain the so-called *natural* boundary conditions. From the arbitrariness of δB_r at $z = \pm L$ and of δB_z at $r = a$ the condition $J_\theta = \lambda B_\theta/2$ follows over the whole surface of the vessel. The arbitrariness of δB_z at the electrodes (which is due to the fact that the total field is the sum of the external field plus the contribution of the plasma) leads to the condition $\gamma = \lambda\Phi/\mu_0$. Here, Φ should be set equal to the value of the potential at the electrodes $\Phi(\pm L) = \mp V/2$. However, defining the potential near the electrodes is difficult due to the limitations of the stationary magnetohydrodynamic (MHD) model employed in this study. This model cannot account for the voltage drop at the sheath, which forms next to the electrodes due to charge separation and other effects associated with a finite flow velocity. If the usual values of the potential on the electrodes ($V \sim 100$ V) are introduced in the condition $\gamma = \lambda\Phi/\mu_0$, for realistic values of the resistivity ($\eta \sim 10^{-6}$ Ωm), the resulting solutions show a huge z-current I_z, which is much larger than the values observed in the experiments. Hence, we will consider a different value $V_0 \ll V$ in the natural boundary condition for γ, chosen according to a global Ohm's law that links the value of the external current to the potential difference between $z = L$ and $z = -L$. As we will show later, such a global Ohm's law follows from the natural boundary conditions at $r = a$. Hence, it appears as a consequence of the variational principle with the constraints employed in (2.1), and should not be considered as an additional condition.

We interpret V_0 as the potential inside the thin layer where separation of charge occurs, i.e. the value of the potential after the fall occurring near the electrodes. For the homogeneous resistivity considered, Ohm's law is assumed to be valid only on the bulk of the plasma and not in the zone close to the electrodes. A possible way to improve the model without abandoning the general framework of the MHD

https://doi.org/10.1017/S0022377805004113 Published online by Cambridge University Press

model is to consider a non-uniform resistivity as in Farengo and Sobehart (1994). However, this complicates the analytical treatment considerably.

In addition to the natural boundary conditions, we will consider the physical ones, $\mathbf{B}\cdot\hat{n}=0$ and $\mathbf{J}\cdot\hat{n}=0$, at $r=a$, and also at the surfaces $z=\pm L$ for $r>b$, in order to model a flux conserver covered on the inside by a dielectric layer. It is worth mentioning that it is possible to include additional constraints in W that make the physical boundary conditions appear as natural conditions coming from the variational principle. The inclusion of such terms in W does not modify the resulting differential equations for $\mathbf{J}$ and $\mathbf{B}$.

We solve (2.3) and (2.4) together with Ampere's law and $\nabla\cdot\mathbf{B}=0$.

In order to simplify the presentation we normalize the different variables and parameters to obtain dimensionless quantities:

$$\begin{gathered}\mathbf{r}/a\to\mathbf{r},\quad \lambda a\to\lambda,\\ \mathbf{B}/|\mathbf{B}_{\rm ext}|\to\mathbf{B},\quad \mathbf{J}\mu_0 a/|\mathbf{B}_{\rm ext}|\to\mathbf{J},\\ \mu_0^2 a\gamma/(\eta|\mathbf{B}_{\rm ext}|)\to\gamma,\quad \frac{V\mu_0}{B_{\rm ext}\eta_0}\to V,\\ b/a\to b,\quad L/a\to L.\end{gathered}\tag{2.5}$$

In terms of the new variables, Ampere's law becomes $\nabla\times\mathbf{B}=\mathbf{J}$, while the rest of the equations remain unchanged.

By generalizing the treatment of the homogeneous Helmholtz equation in Morse and Feshbach (1953), it is possible to write the general solution for $\mathbf{J}$ and $\mathbf{B}$ as

$$\begin{aligned}\mathbf{J}&=\xi+\mu_l\nabla\gamma,\\ \mathbf{B}&=\xi/\lambda+\mu_l\nabla\times(\tilde{\gamma}\hat{z}+f(r)\hat{z})+\nabla\chi,\end{aligned}\tag{2.6}$$

where

$$\xi=\nabla\times(\psi\hat{z})+\frac{1}{\lambda}\nabla\times\nabla\times(\psi\hat{z}),\tag{2.7}$$

$$\nabla^2\chi=0.\tag{2.8}$$

The parameter μ_l is defined as $\mu_l=\mu_0 a/(2\eta\lambda)$ (in terms of the original, not scaled parameters) and ψ satisfies the Helmholtz equation $\nabla^2\psi+\lambda^2\psi=0$. The functions $\tilde{\gamma}$ and $f(r)$ are defined as

$$\tilde{\gamma}=\int_{-L}^{z}\gamma(r,z')\,dz'\tag{2.9}$$

$$f(r)=-\int_0^r dr_2\frac{1}{r_2}\int_0^{r_2} r_1\gamma_z(r_1,-L)\,dr_1,\tag{2.10}$$

where $\gamma_z=\partial_z\gamma$.

Hence, the problem is reduced to finding the solutions for ψ,γ and χ satisfying the desired boundary conditions, which can be written in terms of linear combinations of derivatives of these functions equated to zero. In the general case, the solutions for ψ,γ and χ are Fourier–Bessel series. The function $f(r)$ should be computed for every term in the series for γ.

https://doi.org/10.1017/S0022377805004113 Published online by Cambridge University Press

Note that χ contributes to the magnetic field with the irrotational term $\nabla\chi$ (see (2.6)), which represents the external magnetic field, originating from currents which are outside the vessel. The external magnetic field is assumed to be uniform on the electrodes, normal to them, and with modulus equal to one (because of the scaling considered). However, as indicated above, the magnetic field on the electrodes will also have a contribution coming from the plasma currents (through ψ and γ) and, in general, it will be non-uniform and have non-zero tangent components.

3. Solutions for $b = 1$

When the electrodes cover the whole $z = \pm L$ surfaces, the solutions for γ and χ are simple linear functions, and only ψ has to be written as a Fourier–Bessel series.

The boundary conditions employed are:

$$B_r(1,z) = 0, \quad J_r(1,z) = 0, \quad J_\theta(1,z) = \frac{\lambda}{2} B_\theta(1,z), \tag{3.1}$$

$$\nabla\chi(r,\pm L)\cdot\hat{n} = 1, \quad \gamma(r,\pm L) = \mp\lambda V_0/2, \quad J_\theta(r,\pm L) = \frac{\lambda}{2} B_\theta(r,\pm L). \tag{3.2}$$

3.1. Solution with azimutal symmetry

The solution for the minimum dissipation states with azimutal symmetry given in terms of ψ, γ and χ are:

$$\psi = A_0 J_0(\lambda r) + \sum_{i=1}^{\infty} 2A_i \cosh(k_i z) J_0(k_i' r) \tag{3.3}$$

$$\gamma = C_0 z \tag{3.4}$$

$$\chi = z, \tag{3.5}$$

where k_i' is the ith positive zero of $J_1(x)$ and $k_i'^2 = \lambda^2 + k_i^2$. The constants A_i and C_0 are given by

$$\begin{gathered} A_i = \frac{\mu_l \lambda^2 V_0}{L J_2^2(k_i') \cosh(k_i L)} \int_0^1 \left[r - \frac{J_1(\lambda r)}{J_1(\lambda)} \right] J_1(k_i' r) r \, dr, \quad i \geqslant 1 \\ A_0 = \mu_l \lambda V_0 / [4 L J_1(\lambda)], \\ C_0 = \lambda V_0 / (2L). \end{gathered} \tag{3.6}$$

The value of λ is determined by imposing the helicity balance condition as we will indicate later.

In order to show how the mentioned global Ohm's law appears as a consequence of the natural boundary conditions we go back to the calculations that lead us to the final results for the constants indicated above. From the boundary condition $J_\theta(1,z) = \frac{1}{2}\lambda B_\theta(1,z)$ it follows that $A_0 = \mu_l C_0 / 2 J_1(\lambda)$. Then, the total external current, which in principle depends on A_0 and C_0, can be written in terms of C_0 as

$$I_z \equiv \int_0^1 J_z(r,L) 2\pi r \, dr = 2\pi \mu_l C_0. \tag{3.7}$$

https://doi.org/10.1017/S0022377805004113 Published online by Cambridge University Press

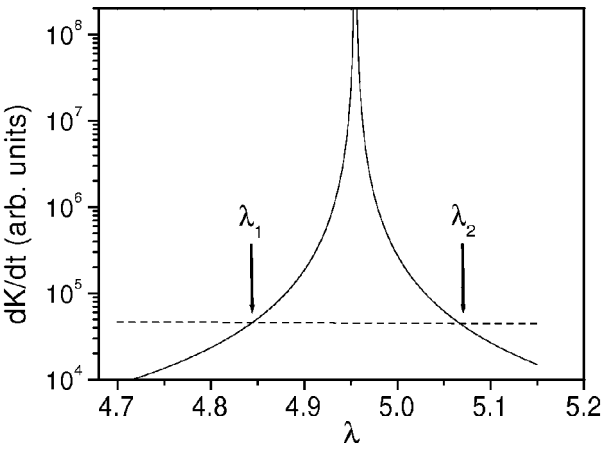


Figure 2. Helicity dissipation rate (solid line) and helicity injection rate (dashed line) as a function of λ, for $a = 0.33$ m, $L = 0.5a$, $B_{\rm ext} = 0.005$ T, $I_z = 6 \times 10^4$ A, $\eta = 3.0 \times 10^{-6}$ Ωm and $V = 100$ V.

Finally, the condition $\gamma(r, \pm L) = \mp \lambda V_0/2$ leads us to the value of C_0 indicated in (3.6). Equating both results for C_0 we obtain Ohm's law,

$$V_0 = \frac{I_z \eta L}{\pi}. \tag{3.8}$$

With this equation we determine the value of V_0 given the desired values of I_z, η and L.

The value of λ is determined by imposing the helicity balance condition for which, following the usual definition of helicity injection in experiments (see Jarboe 1994; Bellan 2000), the true value of the potential on the electrodes (V) is considered.

In the calculations we have considered parameters similar to those proposed for the 'Proto-Sphera' confinement configuration (see Alladio et al. 2000), which has also been considered in Farengo and Caputi (2002) for numerical calculations. Moreover, we have analyzed different values for L and η in the ranges $0.5a \leqslant L \leqslant 1.3a$ and $10^{-6} \leqslant \eta \leqslant 3 \times 10^{-5}$ Ωm, which are of experimental interest. In Fig. 2 we show the curves for the helicity dissipation rate (solid line) and the helicity injection rate (dashed line) as a function of λ, for the original (not scaled) parameters: $a = 0.33$ m, $L = 0.5a$, $B_{\rm ext} = 0.005T$, $I_z = 6 \times 10^4$ A, $\eta = 3 \times 10^{-6}$ Ωm and $V = 100$ V.

In general, when helicity balance is imposed for a given set of the external parameters, two different solutions corresponding to two different values of λ are obtained. In Fig. 2 we have indicated the values of λ_1 and λ_2 where helicity injection and dissipation are equal. The solution with the lower value of λ (λ_1) corresponds to a spheromak with internal flux, while the other is a spheromak with external flux. In Fig. 3 we show the flux contours of the poloidal magnetic field for the solutions with internal flux (Fig. 3(a)) and external flux (Fig. 3(b)) for the same parameters indicated in Fig. 2.

Returning to Fig. 2, it can be seen that there is a critical value (λ_0) of the eigenvalue where the helicity dissipation rate diverges. We have observed that the value of λ_0 depends on L but not on η. For the parameters of Fig. 2 we have $\lambda_0 \sim 4.95$. At that value of λ, the total toroidal current also diverges, and changes

https://doi.org/10.1017/S0022377805004113 Published online by Cambridge University Press

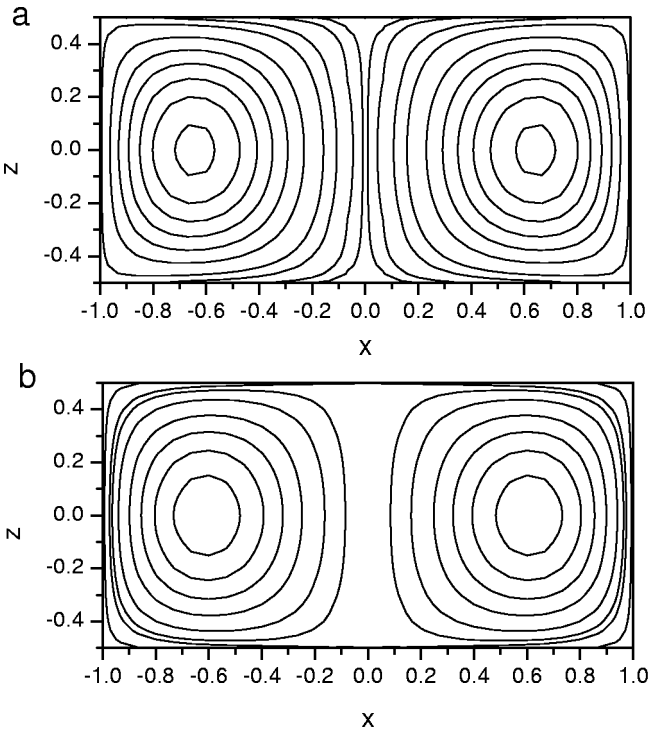


Figure 3. Poloidal flux contours for spheromak solutions with (a) internal and (b) external flux. The parameters are the same as in Fig. 2.

of sign (it goes from $+\infty$ for $\lambda < \lambda_0$ to $-\infty$ for $\lambda > \lambda_0$); accordingly, the solution changes from having internal flux to have external flux. It should be mentioned, that the helicity injection rate is not exactly a constant as it may seem to be in Fig. 2 due to the scale employed. Actually, it grows monotonically with λ due to changes in the contribution of the plasma to the total magnetic flux on the electrodes.

For the different sets of parameters studied we have found that the solution with internal flux (with helicity balance), which is of the kind commonly observed in experiments, has a lower energy dissipation rate than the solution with external flux (differing typically by 10%). Hence, the solution with internal flux is expected to be the most stable one. Furthermore, we note that only this solution is properly an FCS.

In Fig. 4(a) we show B_θ and B_z as a function of r at $z = 0$ for the spheromak with internal flux shown in Fig. 3(a). It can be seen that B_θ does not vanish at $r = a$, as there is a finite current I_z circulating through the electrodes. In Figs 4(b) and (c) we respectively show J_θ and $\mathbf{B}\cdot\mathbf{J}/B^2$ as functions of r at $z = 0$ for the same solution. In contrast to what occurs in the force-free solution of Taylor (1974) for the minimum-energy states, here $\mathbf{B}\cdot\mathbf{J}/B^2$ does depend on r. However, its value is always close to λ, which is indicated with a dotted line. (In Taylor's theory $\mathbf{B}\cdot\mathbf{J}/B^2$ is constant and equal to the eigenvalue λ_{T}, that satisfies $\nabla\times\mathbf{B} = \lambda_{\mathrm{T}}\mathbf{B}$.) The total toroidal current of the solution is $I_\theta = 2.43\times10^5$ A, which is of the order of the value expected for Proto-Sphera ($I_\theta \sim 2.5\times10^5$ A).

https://doi.org/10.1017/S0022377805004113 Published online by Cambridge University Press

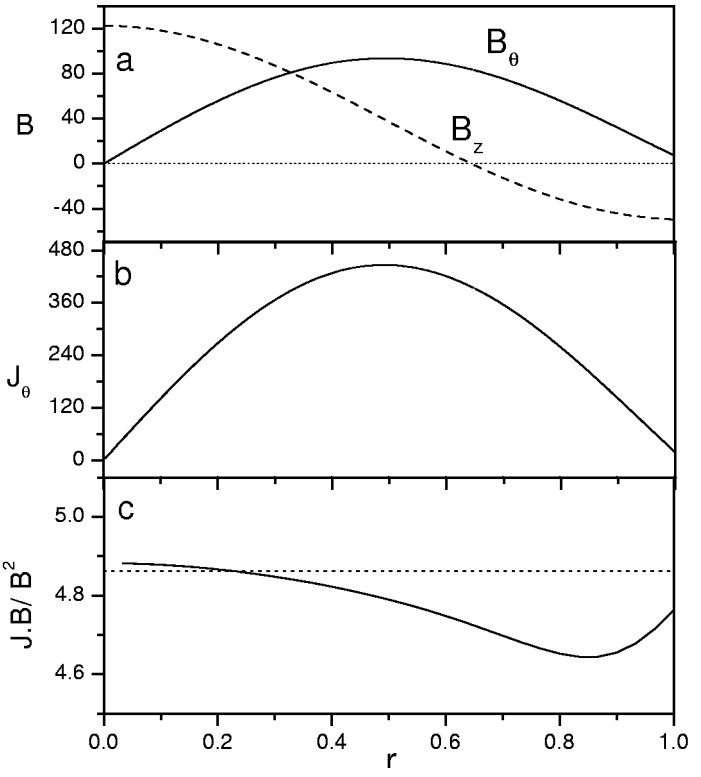


Figure 4. Profiles of (a) B_z and B_θ; (b) J_θ and (c) $\mathbf{B}\cdot\mathbf{J}/B^2$ as a function of r at $z = 0$ for the solution with internal flux. In (c) the dotted line indicates the value of λ. The parameters are the same as in Fig. 2.

We have studied the minimum-energy dissipation states for different sets of parameters in the region of interest. In Fig. 5(a) we show the values of λ_1 and λ_2 as a function of the resistivity. In Fig. 5(b) we show the toroidal current I_θ for the corresponding solutions. It can be seen that I_θ decreases with η for both solutions (in absolute value).

As the aspect ratio of the vessel is variated, the general characteristics of the two spheromak solutions remain unchanged. In Fig. 6 we display the flux contours of the poloidal magnetic field for minimum dissipation states with $L = 1.3$, which is the aspect ratio of the proposed Proto-Sphera device. In Fig. 7 we show the profiles of B_θ, B_r, J_θ and $\mathbf{B}\cdot\mathbf{J}/B^2$ for the solution with internal flux at $z = 0$. The total toroidal current of the FCS is $I_\theta = 3.8 \times 10^5$ A in this case, which is slightly higher than the value obtained for $L = 0.5$ and expected for Proto-Sphera.

In all the cases studied we have verified that there is an appropriate balance of injected and dissipated power. For the value of $V = 100$ V considered, the ratio of the dissipated power (by the Ohmic mechanism) to the injected power, is always very close to 3/4. We assume that the remaining power is lost through processes not included in the resistive MHD model employed. If lower values of V are considered the ratio increases until it reaches unphysical values greater than one. For instance, this occurs for $V \sim 60$ V for the parameters considered in Fig. 2.

https://doi.org/10.1017/S0022377805004113 Published online by Cambridge University Press

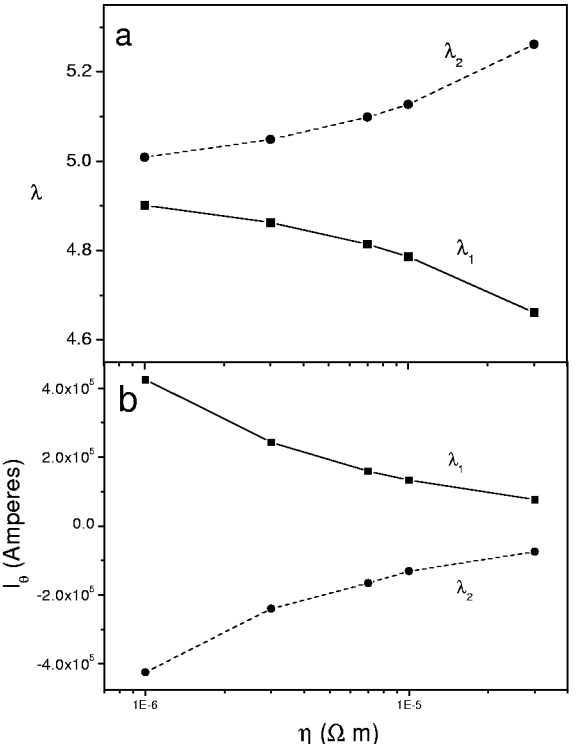


Figure 5. (a) Eigenvalues λ_1 and λ_2 as a function of the resistivity. (b) Toroidal current of the corresponding solutions. The other parameters are the same as in Fig. 2.

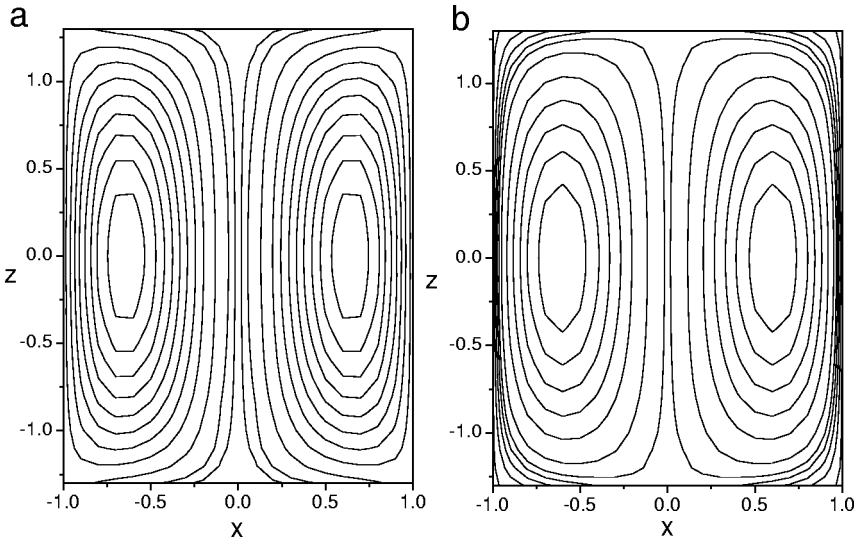


Figure 6. Poloidal flux contours for the spheromak solutions with (a) internal and (b) external flux. The parameters are the same as in Fig. 2, except for the aspect ratio of the vessel which in this case is $L = 1.3$.

https://doi.org/10.1017/S0022377805004113 Published online by Cambridge University Press

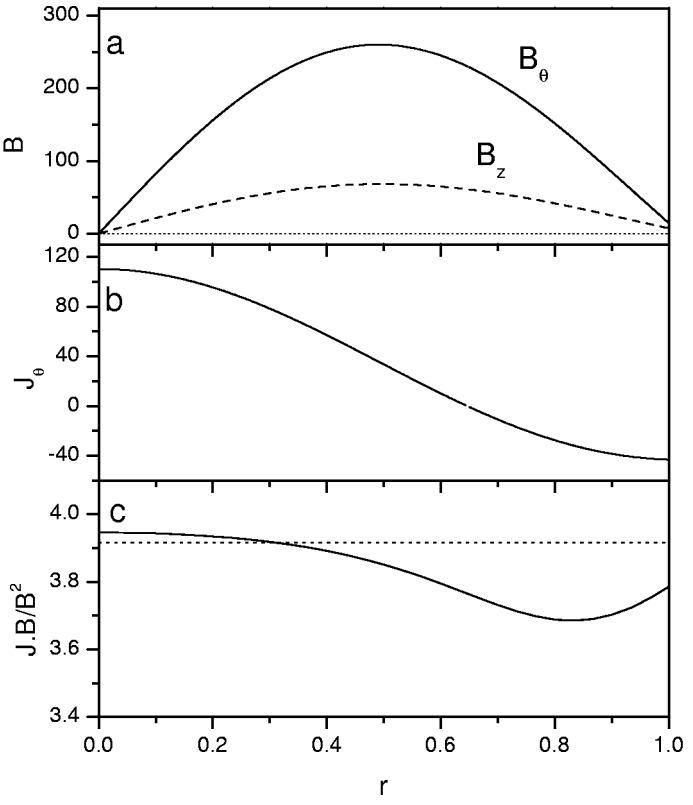


Figure 7. Profiles of (a) B_z and B_θ; (b) J_θ and (c) $\mathbf{B}\cdot\mathbf{J}/B^2$ as a function of r at $z = 0$ for the solution with internal flux. In (c) the dotted line indicates the value of λ. The parameters are the same as in Fig. 6.

All the results in Figs 2–6 are computed by summing up three terms on the expansion for ψ. We have verified that this represents a very good approximation to the whole series.

We want to mention here a last fact concerning boundary conditions. Exactly the same solutions presented above are obtained if, instead of considering the natural boundary condition $\gamma = \lambda\Phi$, one asks for a uniform J_z on the electrodes with the desired value of the integral I_z. In that case, the resulting γ function is homogeneous on the electrodes and its value is $\lambda V_0/2$, with V_0 defined from Ohm's law (3.8) for that I_z.

3.2. θ-dependent solutions

We have also calculated non-axisymmetric solutions for minimum dissipation states, with a sinusoidal dependence on θ. We consider a perturbation to the axisymmetric state with no contribution to I_z nor to the total magnetic flux through the electrodes, and satisfying $\mathbf{J}_1(1,z)\cdot\hat{n} = 0$ and $\mathbf{B}_1(1,z)\cdot\hat{n} = 0$. The solution is given by

$$\psi_1 = J_1(qr)\cos(q'z+\theta), \quad \gamma_1 = -sI_1(qr)\sin(qz+\theta), \quad \chi_1 = 0. \tag{3.9}$$

These functions should be summed to the axisymmetric ones weighted by an arbitrary amplitude (equal for both ψ an γ). The constants q and s_1 are determined

https://doi.org/10.1017/S0022377805004113 Published online by Cambridge University Press

from the conditions at $r = 1$, while $q'^2 = \lambda^2 - q^2$. We have observed for several different values of the parameters V, η and I_z that this kind of non-axisymmetric perturbation always increases the total energy dissipation. Hence, the axisymmetric solution appears to be the more stable one from the point of view of the minimum-energy dissipation principle.

4. Solutions for $b < 1$

Now we turn to study the case where the electrodes do not cover the entire $z = \pm L$ surfaces. In this case the solutions for all the functions γ, χ and ψ result in Fourier–Bessel series. For $b < 1$ there is a difficulty associated with the natural boundary condition $\gamma = \lambda\Phi/2$, since it should only be imposed for $r < b$ (on the $z = \pm L$ surfaces) and there is not an obvious condition for γ for $r > b$. Note that δB_z on $z = \pm L$ should be considered arbitrary only for $r < b$. Hence, the natural condition for γ is given only for $r < b$. In contrast δB_r is still arbitrary over the entire boundary of the vessel, implying $J_\theta = \lambda B_\theta/2$. In order to fix the boundary condition for γ, one possibility is to interpret $\nabla\gamma$ as an electric field and to impose $\nabla\gamma \cdot \hat{n} = 0$ for $r > b$ on $z = \pm L$. However this mixed (Neumann–Dirichlet) condition is not easy to handle analytically. Hence, we have adopted the alternative mentioned at the end of the last section which is to fix the total current on the electrodes assuming a uniform value of J_z on them. The resulting boundary conditions considered are:

$$B_r(1, z) = 0, \quad J_r(1, z) = 0, \quad J_\theta(1, z) = \frac{\lambda}{2} B_\theta(1, z),$$

$$\nabla\chi(r, \pm L) \cdot \hat{n} = \pm H(b - r), \quad J_z(r, \pm L) = \frac{I_0 H(b - r)}{\pi b^2}, \quad J_\theta(r, \pm L) = \frac{\lambda}{2} B_\theta(r, \pm L),$$

where $H(x)$ is the Heaviside function and I_0 is the total current on the electrodes expressed in non-dimensional form according to the scaling for $\mathbf{J}$ and $\mathbf{r}$ in equation (2.5).

The solution is

$$\psi = A_0 J_0(\lambda r) + \sum_{i=1}^{\infty} 2A_i \cosh(k_i z) J_0(k_i' r) \tag{4.1}$$

$$\gamma = C_0 z + \sum_{i=1}^{\infty} 2C_i \sinh(k_i' z) J_0(k_i' r) \tag{4.2}$$

$$\chi = E_0 z + \sum_{i=1}^{\infty} 2E_i \sinh(k_i' z) J_0(k_i' r), \tag{4.3}$$

where k_i' is the ith positive zero of $J_1(x)$ and $k'^2 = \lambda^2 + k^2$. The constants A_i, C_i and E_i are given by

$$A_0 = \frac{I_0}{4\pi J_i(\lambda)}, \quad C_0 = \frac{I_0}{2\pi\mu_l}, \quad E_0 = b^2, \tag{4.4}$$

$$A_i = \frac{R_i - a_{2i} C_i}{a_{i1}} \quad \text{for } i > 0 \tag{4.5}$$

https://doi.org/10.1017/S0022377805004113 Published online by Cambridge University Press

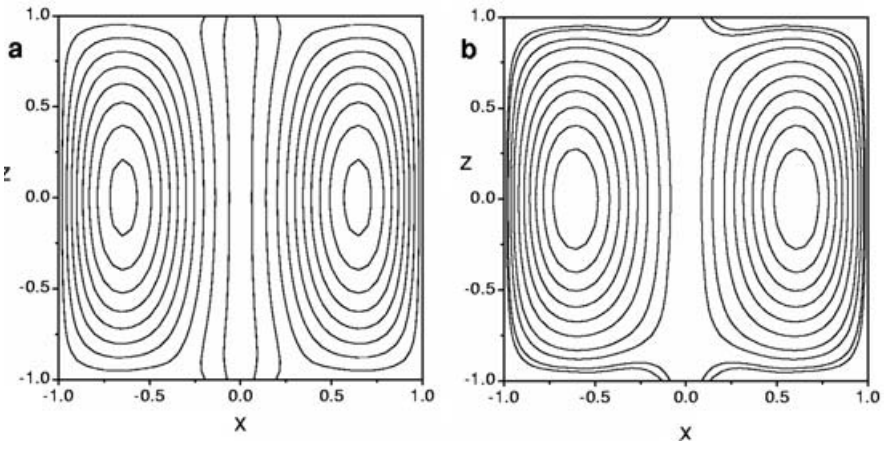


Figure 8. Poloidal flux contours of the minimum dissipation states for a system with electrode radius $b = 0.2a$. (a) Solution with internal flux ($\lambda \simeq 4.015$) and (b) solution with external flux ($\lambda \simeq 4.2705$).

$$C_i = \frac{Q_i a_{1i} - R_i a_{3i}}{a_{4i} a_{1i} - a_{2i} a_{3i}} \quad \text{for } i > 0 \tag{4.6}$$

$$E_i = \frac{b(J_1(bk_i') - J_1(k_i'))}{J_0^2(k_i') k_i'^2 \cosh(k_i' L)} \quad \text{for } i > 0, \tag{4.7}$$

where

$$R_i = \frac{1}{J_0^2(k_i')} \left[\int_0^1 (J_z(r, L) - \mu_l C_0 - \lambda A_0 J_0(\lambda)) J_0(k_i' r) r \, dr \right] \tag{4.8}$$

$$Q_i = \frac{\lambda I_0(k_i'^2 J_0(k_i') + k_i^2 J_2(k_i'))}{4Pi J_2^2(k_i') k_i k_i'^2}, \tag{4.9}$$

$$a_{1i} = \frac{k_i'^2 \cosh(k_i L)}{\lambda}, \quad a_{2i} = \mu_l k_i' \cosh(k_i' L) \tag{4.10}$$

$$a_{3i} = k_i' \cosh(k_i L), \quad a_{4i} = \mu_l \lambda \cosh(k_i' L). \tag{4.11}$$

Given a set of external parameters, as in the case with $b = 1$, spheromak solutions with internal and external flux are obtained. In Fig. 8 we show the contours of the poloidal magnetic field of both solutions for a device with $b = 0.2$ and $L = 1$. The rest of the parameters in the original dimensions are: $I_z = 6 \times 10^4$ A, $a = 0.33$ m, $V = 100$ V, $\eta = 3 \times 10^{-6}$ Ωm and $B_{\text{ext}} = 0.125$ T. The value of B_{ext} was chosen to obtain the same external magnetic flux as in the solutions presented for $b = 1$. In Fig. 9 we show B_θ, J_θ and $\mathbf{J} \cdot \mathbf{B}/B^2$ as a function of r at $z = 0$ for the solution with internal flux. The resulting total toroidal current for this solution is $I_z = 3.43 \times 10^5$ A. The ratio of the dissipated power to the injected power is about 3/4 as in the solutions for $b = 1$. All the results presented for $b < 1$ were obtained including four terms in the series for ψ, γ and χ.

https://doi.org/10.1017/S0022377805004113 Published online by Cambridge University Press

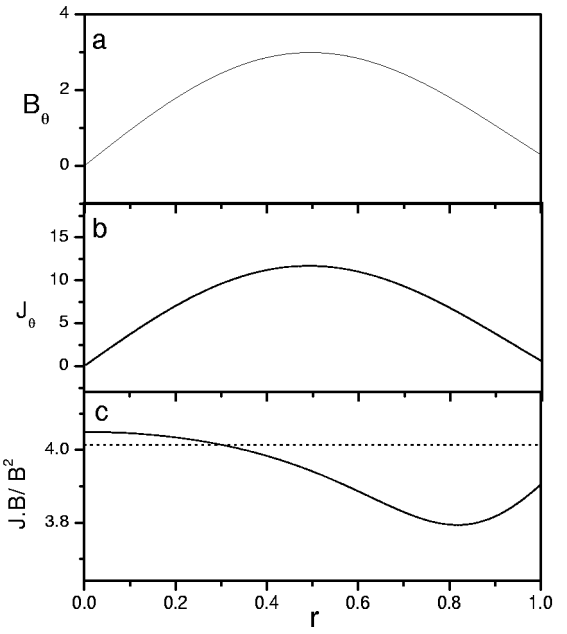


Figure 9. (a) Toroidal magnetic field, (b) toroidal current and (c) $\mathbf{J}\cdot\mathbf{B}/B^2$ for $z = 0$ for the solution with internal flux of Fig. 8(a).

5. Summary, discussion and conclusions

In this paper we have presented analytical solutions for FCS configurations sustained by helicity injection in cylindrical vessels, which are obtained as minimum-energy dissipation states. We have analyzed different values of the parameters (the resistivity and the aspect ratio) over a range of experimental interest.

First, we have studied in detail the case where the electrodes cover the entire plane surfaces of the vessel. In that case we began by presenting the solutions with azimutal symmetry and studied them for different values of the parameters. Also, we have presented non-symmetric solutions that result in higher dissipation rates (for all the parameters analyzed), and hence, from the point of view of the minimum dissipation principle, are viewed as being more unstable than solutions with azimutal symmetry. After that, we have presented the analytical solutions with azimutal symmetry for the case where the radius of the electrodes is smaller than that of the vessel. In all the cases, the parameters considered in the calculations and also those obtained from the solutions, are compatible with those expected in experimental devices.

In the case of equal radius of the vessel and the electrodes, we have observed an interesting result: the appearance of an Ohm's law as a consequence of the variational principle. This relation links the total current I_z to the potential difference between the extremes of the vessel. Unfortunately, for realistic values of I_z and η, the potential difference predicted is much lower than that expected for experiments. (Or, inversely, for realistic values of $\Delta\Phi$, the current obtained is much larger than the expected one.) This lead us to consider two different values of the potential: $V \sim 100$ V, which is considered as the real value of the potential on the electrodes and is used to compute the helicity injection rate, and $V_0 < V$, which is the one that

https://doi.org/10.1017/S0022377805004113 Published online by Cambridge University Press

cancels the surface term on the functional derivative on the variational principle and is considered as the effective difference of potential sustained on the plasma at $\pm L$. We have further interpreted the difference between V and V_0 as the potential drop occurring close to the electrodes as a consequence of charge separation and other phenomena that are beyond the framework of MHD. We note that if the surface term on the variational principle had been ignored, as is sometimes done in the literature, this problem would have not been observed and everything could have been done without mention to V_0. The need to consider two potentials is a limitation of the MHD model, that could may be partially avoided by considering inhomogeneous resistivity. However, this forbids the possibility of having an exact analytical treatment.

We expect that the analytical solutions presented could be used as a basis for further studies on stability and decay of spheromaks. Also, more detailed numerical models may contribute to adjusting and improving the solutions in the region close to the electrodes.

References

Alladio, F. et al. 2000 Proto-Sphera. CR-ENEA Frascati.
Bellan, P. M. 2000 *Spheromaks*. London: Imperial College Press.
Caputi, K. I. and Farengo, R. 2001 *Plasma Phys. Control. Fusion* **43**, 795.
Farengo, R. and Caputi, K. I. 2002 *Plasma Phys. Control. Fusion* **44**, 1–16.
Farengo, R. and Sobehart, J. R. 1993 *Plasma Phys. Control. Fusion* **35**, 465.
Farengo, R. and Sobehart, J. R. 1994 *Plasma Phys. Control. Fusion* **36**, 1691.
Hameiri, E. and Bhattacharjee, A. 1987 *Phys. Rev.* A **35**, 768.
Jarboe, T. R. 1994 *Plasma Phys. Control. Fusion* **36**, 945.
Montgomery, D. and Phillips, L. 1988a *Phys. Rev.* A **38**, 2953.
Montgomery, D. and Phillips, L. 1988b *Physica* D **37**, 215.
Morse, P. and Feshbach, H. 1953 *Methods of Theoretical Physics*. New York: McGraw-Hill.
Taylor, J. B. 1974 *Phys. Rev. Lett.* **33**, 1139.
Wang, C. Y. and Bhattacharjee, A. 1991 *Phys. Fluids* B **3**(12), 3462.

https://doi.org/10.1017/S0022377805004113 Published online by Cambridge University Press